How to cite: Angew. Chem. Int. Ed. 2024, e202319981
doi.org/10.1002/anie.202319981

Chemoradiotherapy

Phosphate Coordination to Metal-Organic Layer Secondary Building Units Prolongs Drug Retention for Synergistic Chemoradiotherapy

*Taokun Luo[+], Xiaomin Jiang[+], Jinhong Li[+], Geoffrey T. Nash, Eric Yuan, Luciana Albano, Langston Tillman, and Wenbin Lin**

Abstract: Chemoradiotherapy combines radiotherapy with concurrent chemotherapy to potentiate antitumor activity but exacerbates toxicities and causes debilitating side effects in cancer patients. Herein, we report the use of a nanoscale metal-organic layer (MOL) as a 2D nanoradiosensitizer and a reservoir for the slow release of chemotherapeutics to amplify the antitumor effects of radiotherapy. Coordination of phosphate-containing drugs to MOL secondary building units prolongs their intratumoral retention, allowing for continuous release of gemcitabine monophosphate (GMP) for effective localized chemotherapy. In the meantime, the MOL sensitizes cancer cells to X-ray irradiation and provides potent radiotherapeutic effects. GMP-loaded MOL (GMP/MOL) enhances cytotoxicity by 2-fold and improves radiotherapeutic effects over free GMP in vitro. In a colon cancer model, GMP/MOL retains GMP in tumors for more than four days and, when combined with low-dose radiotherapy, inhibits tumor growth by 98%. The synergistic chemoradiotherapy enabled by GMP/MOL shows a cure rate of 50%, improves survival, and ameliorates cancer-proliferation histological biomarkers.

Traditional chemotherapy targets fast-proliferating tumor cells using cytotoxic drugs,[1] but most chemotherapeutics have narrow therapeutic indices because of their nonspecific distribution to normal organs.[2] Localized chemotherapy has been developed to reduce systemic side effects,[3] which has proven effective for some tumors, including bladder and liver cancer.[4] However, localized chemotherapy is limited by poor retention of small-molecule drugs in tumors.[5] Maintaining intratumoral drugs above therapeutic concentrations over a period of time is crucial to achieving optimal treatment outcomes.

Radiotherapy (RT) is another widely used cancer treatment that utilizes ionizing radiation to kill malignant cells.[6] Despite extensive research on radiosensitization over the past century, non-toxic radiosensitizers have not been approved by the Food and Drug Administration for cancer treatment.[7] Some chemotherapeutics are used in combination with RT to enhance antitumor effects,[8] but these chemoradiotherapy regimens exacerbate the toxicities of both modalities, leading to debilitating side effects in cancer patients.[9] Thus, there is a need for novel strategies to simultaneously control the release of chemotherapeutics in tumors and enhance the antitumor activity of RT.

Metal–organic frameworks (MOFs) have recently been examined for biomedical applications.[10] In particular, MOFs consisting of high-Z-metal-based secondary building units (SBUs) and photosensitizing ligands have been demonstrated as efficient non-toxic radiosensitizers via a unique radiotherapy-radiodynamic therapy (RT-RDT) process.[11] We have recently shown that the dimensional reduction of 3D MOFs to 2D metal-organic layers (MOLs) further improves the RT-RDT efficiency by increasing energy-transfer efficiency and enhancing the diffusion of reactive oxygen species.[12] Furthermore, 2D MOLs possess more accessible binding sites than 3D MOFs, allowing for facile conjugation of therapeutic molecules via post-synthetic functionalization.[13]

Antimetabolite chemotherapeutics such as gemcitabine and 5-fluorouracil are converted to their active triphosphates to exert antitumor effects, with the conversion to their monophosphates as the rate-limiting step.[14] As a result, gemcitabine monophosphate (GMP) is much more potent than gemcitabine but is quickly cleared from tumors due to its hydrophilicity. We hypothesized that GMP could be loaded on MOL SBUs for slow release in tumors and to enhance the RT effects.[13c,d] Herein, we report the conjugation of GMP to the SBUs of a 2D MOL comprising Hf_{12}-SBUs and Ir-based photosensitizing ligands for synergistic chemoradiotherapy.

We first synthesized the 2D MOL via a solvothermal reaction between $HfCl_4$ and $Ir(DBB)[dF(CF_3)ppy]^{2+}$ [DBB = 4,4′-di(4-benzoato)-2,2′-bipyridine; $dF(CF_3)ppy$ = 2-(2,4-difluorophenyl)-5-(trifluoromethyl)pyridine] in *N,N*-dimethylformamide as previously reported.[12b] GMP was loaded onto the MOL by stirring a mixture of GMP and

[*] T. Luo,[+] X. Jiang,[+] J. Li,[+] G. T. Nash, E. Yuan, L. Albano, L. Tillman, Prof. Dr. W. Lin
Department of Chemistry, The University of Chicago, Chicago, IL 60637 (USA)
E-mail: wenbinlin@uchicago.edu
Prof. Dr. W. Lin
Department of Radiation and Cellular Oncology and Ludwig Center for Metastasis Research, The University of Chicago, Chicago, IL 60637 (USA)
[+] These authors contributed equally

MOL in ethanol/water at one GMP per Hf_{12}-SBU at room temperature for 15 minutes, followed by washing with water to afford GMP/MOL. Two control samples, DPPA/MOL and PPA/MOL, were similarly prepared with diphenylphosphinic acid (DPPA) and phenylphosphonic acid (PPA) instead of GMP to study their interactions with SBUs. ^{1}H and ^{31}P NMR signals of GMP, DPPA, and PPA in D_2O disappeared after conjugation to the MOL (Figures S2 and S3) due to decreases in tumbling rates upon coordination to Hf_{12} SBUs.[15] This result suggests the coordination of GMP to the Hf_{12}-SBU.

Transmission electron microscopy (TEM) showed unchanged nanosheet morphology upon conjugating GMP, DPPA, and PPA to the MOL (Figures 1a–c and S4). Atomic force microscopy (AFM) revealed the monolayer structure of all MOLs but slight increases in thickness from 1.8 nm for the MOL to 1.8, 1.9, and 2.3 nm, respectively, for PPA/MOL, GMP/MOL, and DPPA/MOL. The increases in heights are consistent with increasing sizes of PPA, GMP, and DPPA and support their coordination with Hf_{12}-SBUs (Figures 1d–f and S4). All MOLs exhibited the same crystalline structure with identical powder X-ray diffraction (PXRD) patterns (Figure 1g) and similar ζ-potentials and hydrodynamic sizes with average diameters ranging from 225 nm to 265 nm (Figures 1h and S5). The MOL also showed good chemical, colloidal, and structural stability under physiological conditions (Figure S6).

Solid-state ^{31}P NMR spectroscopy showed broadening and upfield shifts of DPPA, PPA, and GMP signals upon conjugation to the MOL (Figure 2a,b), which supported their coordination with Hf_{12}-SBUs.[16] Density functional theory (DFT) calculations revealed decreases in free energy changes following the order of GMP ($\Delta G = -42.4\ kcal \cdot mol^{-1}$), PPA ($\Delta G = -28.3\ kcal \cdot mol^{-1}$), and DPPA ($\Delta G = -22.8\ kcal \cdot mol^{-1}$) in their substitution for trifluoroacetate (TFA) groups on Hf_{12}-SBUs, indicating the strongest binding between GMP and Hf_{12} SBU (Figure 2c). Isothermal titration calorimetry (ITC) measurements showed that GMP possessed a 1.8 times higher association constant (K_a) than PPA (Figure 2d). DPPA did not show an obvious exotherm during titration. At stoichiometric ratios relative to capping TFA groups, DPPA and PPA showed higher loading efficiencies than GMP (Figure S7).

We hypothesized that the coordinated GMP, DPPA, and PPA on Hf_{12}-SBUs could be released by high concentrations of phosphate ions under certain physiological conditions.

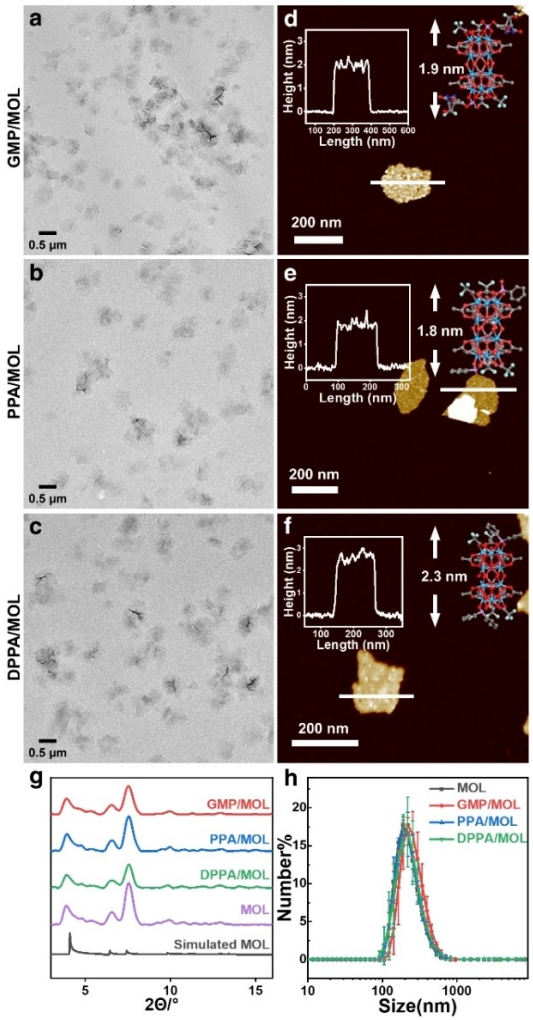

Figure 1. (a–c) TEM images of (a) GMP/MOL, (b) PPA/MOL, (c) DPPA/MOL. (d–f) AFM images of (d) GMP/MOL, (e) PPA/MOL, and (f) DPPA/MOL. (g) PXRD patterns of MOLs and the simulated pattern for the bare MOL. (h) Number-averaged sizes of MOLs in water.

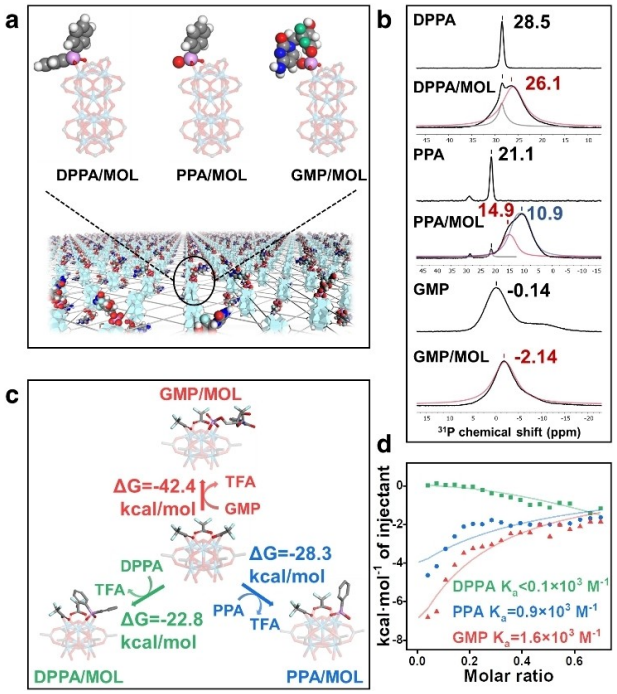

Figure 2. (a) Schematic showing coordination between DPPA, PPA, or GMP and the MOL (ligands were simplified as grey sticks for clarity; white = H; grey = C; red = O; blue = N; green = F; pink = P; cyan = Hf). (b) Solid-state ^{31}P NMR spectra of DPPA, PPA, GMP, and their MOL conjugates. (c) Free energy changes of TFA substitution by DPPA, PPA, or GMP from DFT calculations. (d) ITC results showing binding affinity between the MOL and DPPA, PPA, or GMP.

The release profiles of DPPA/MOL, PPA/MOL, and GMP/MOL were studied by liquid chromatography-mass spectrometry (LC–MS) in 0.1× PBS (1.18 mM phosphate) and 1× PBS (11.8 mM phosphate), which mimic extracellular and intracellular phosphate concentrations, respectively (Figures 3a and S13).[17] At a higher loading ratio, GMP, DPPA, and PPA were more readily released from their MOL conjugates, whereas 10-fold phosphate concentrations increased their release by 1.6-fold (Figure 3b–d). The release rate followed the order of DPPA > PPA > GMP, which correlated with the binding affinity trend from DFT and ITC studies (Figures 2c,d and S12). These results suggest the ability to slowly release small molecule drugs from their MOL conjugates at an elevated phosphate concentration intracellularly.[13c,18]

Based on these findings, we tested if GMP/MOL could slowly release GMP for enhanced anticancer efficacy. Murine colon cancer CT26 cells exhibited similar uptake of MOL and GMP/MOL over 12 hours (Figure 4a). GMP/MOL showed higher cytotoxicity than GMP with 1.87-fold and 1.91-fold lower half maximal inhibitory concentrations (IC_{50}) than free GMP in CT26 and MC38 cells, respectively (Figures 4b and S14, and Table S3). The enhanced cytotoxicity of GMP/MOL is likely due to the increased cellular availability of GMP via endocytosis of GMP/MOL followed by phosphate-triggered release of GMP from GMP/MOL. Additionally, GMP/MOL showed a large therapeutic window with a much lower toxicity to primary cells with slower proliferation and nucleoside-related metabolism (Figure S15).

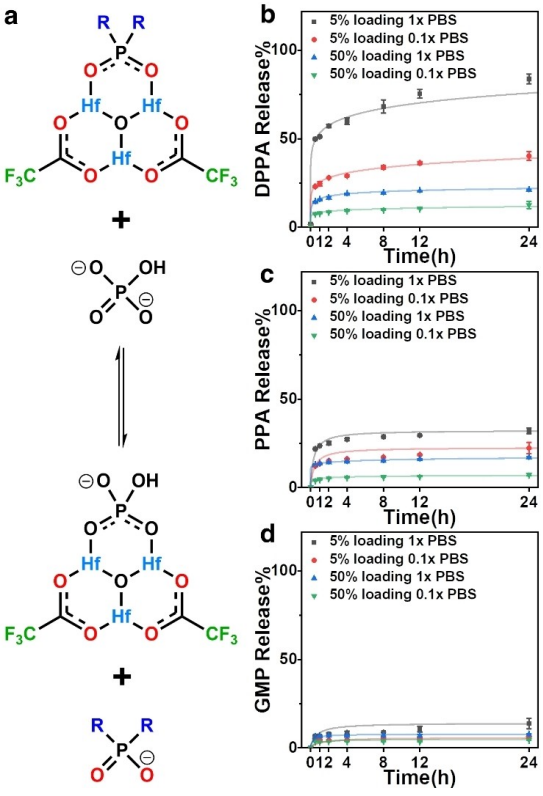

Figure 3. (a) Schematic showing phosphate-dependent release. (b-d) Release percentages of (b) DPPA, (c) PPA, and (d) GMP from the MOL with 5% or 50% of drug loading ratio in 0.1×PBS or 1×PBS, respectively ($n=3$).

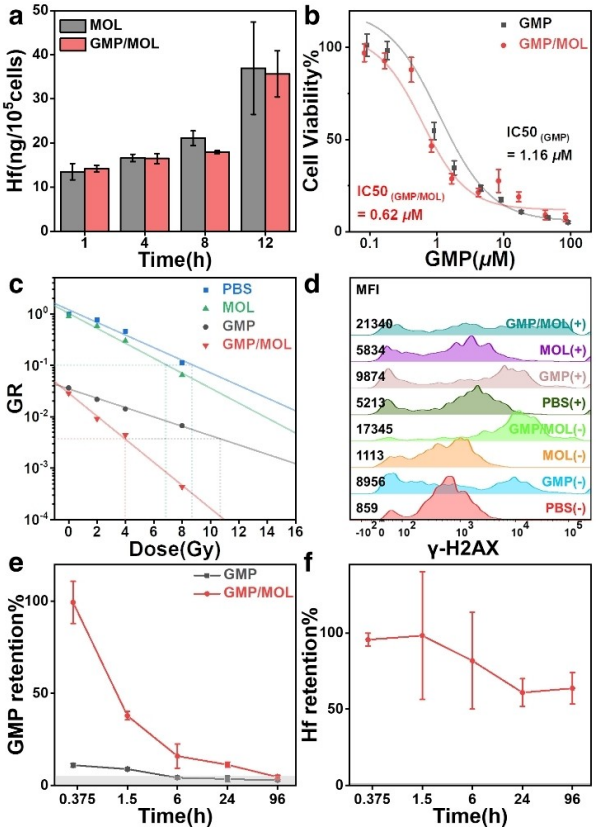

Figure 4. (a) Time-dependent uptake of MOL and GMP/MOL by CT26 cells ($n=3$). (b) Viability of CT26 cells after incubation with free GMP or GMP/MOL for 48 hours ($n=3$). (c) GR assays showing radio-enhancement of MOL, GMP, or GMP/MOL in CT26 cells ($n=3$). (d) Fluorescence histograms showing DNA DSBs quantified with γ-H2AX staining by flow cytometry (MFI, mean fluorescence intensity). (e,f) Tumor retention of (e) GMP (31.4 μg/mouse) and (f) Hf (1 μmol/mouse) after *i.t.* injection of free GMP or GMP/MOL into subcutaneous CT26 tumors ($n=3$. The grey area in (e) indicates the detection limit.

The radiosensitizing effects of the MOL and GMP/MOL were evaluated by growth rate (GR) inhibition assays and immunofluorescence staining of phosphorylated histone H2 A.X (γ-H2AX) in CT26 cells at a GMP concentration of 1.67 μM and a Hf concentration of 20 μM. Compared to radiation alone [PBS(+)], MOL plus X-ray [MOL(+)] treatment showed a steeper X-ray-dose-dependent toxicity with a growth inhibition factor at 10% growth rate ($GIF_{10\%}$) of 1.27 due to the reported RT-RDT effect (Figures 4c and S16).[11a,13c,19] GMP and GMP/MOL had lower starting GR at 0 Gy due to their cytotoxicity against proliferating cancer cells. GMP/MOL(+) outperformed GMP(+) with a $GIF_{10\%}$ of 2.69, which was calculated relative to the GR curve of GMP (Figures 4c and S16–S17). γ-H2AX staining of CT26 nuclei showed that GMP/MOL(+) treatment caused the highest DNA double-strand breaks (DSB), which was 3.66-

fold and 2.16-fold higher than MOL(+) and GMP(+) groups, respectively (Figures 4d and S18).

We then investigated if GMP/MOL could retain GMP in subcutaneous CT26 tumors by LC-MS quantification of GMP and inductively coupled plasma-mass spectrometry (ICP-MS) analysis of Hf. After intratumoral (*i.t.*) injection, GMP was mostly (>88 %) cleared from the tumors within 20 minutes and fell below the detection limit in 6 hours (Figure 4e). In contrast, GMP/MOL retained GMP with a 24.7-fold higher tumor area under curve than free GMP. Approximately 5 % GMP was retained in tumors 4 days post *i.t.* injection (Figure 4e). As this time frame covered all RT fractions, we expected significant synergy between the slowly released GMP and fractionated RT. We further showed that GMP release was not caused by the disintegration of the MOL as >60 % of the MOL was retained in the tumors 4 days post *i.t.* injection (Figure 4f). Steady and low plasma concentrations of GMP and Hf supported the slow release of GMP from GMP/MOL and intratumoral retention of the MOL (Figures S19 and S20). These results show that GMP/MOL is retained in tumors to slowly release GMP and can act as a drug reservoir for antitumor applications.

The antitumor efficacy of GMP/MOL(+) was evaluated in CT26 tumor-bearing BALB/c mice. The mice were *i.t.* injected with saline, GMP, MOL, or GMP/MOL and then irradiated with 2 Gy X-rays per fraction for 3 consecutive days (Figure S21). GMP/MOL(−) moderately inhibited tumor growth by chemotherapeutic effects with a tumor growth inhibition index (TGI) of 0.50. The radiotherapeutic effects of PBS(+) also moderately inhibited tumor growth with a TGI of 0.59. GMP(+) and MOL(+) enhanced RT with TGIs of 0.75 and 0.77, respectively. When GMP and MOL were injected into the tumor squentially, they exhibited a moderate TGI of 0.76. GMP/MOL(+) synergized the chemotherapeutic effects of slowly released GMP and enhanced RT by the MOL to regress tumors with a TGI of 0.98 (Figures 5a, S22, S23 and Table S4). Half of GMP/MOL(+)-treated mice were tumor-free on Day 90 post treatment, while all mice in GMP(+) and MOL(+) groups reached euthanization limit by Day 42 and Day 44, respectively (Figure 5b and Table S5). No apparent body weight loss and organ toxicities were observed during the study (Figures 5c and S24). Immunohistochemistry (IHC) staining of CT26 tumors was performed 24 hours after the last X-ray irradiation to quantify DNA DSBs and the proliferation and apoptosis of cancer cells. While both PBS(+) and GMP(+) increased γ-H2AX-positive cells to 61.4 % and 68.0 % from 15.6 % for PBS(−), MOL(+) and GMP/MOL(+) further increased γ-H2AX-positive cells to 77.5 % and 80.5 % (Figures 5d and S25). GMP/MOL(+) significantly suppressed tumor proliferation with the percentage of Ki67-positive tumor cells 10.6-fold and 16.5-fold lower than GMP(+) and PBS(+) groups, respectively (Figures 5e and S26). Terminal deoxynucleotidyl transferase dUTP nick end labeling (TUNEL) revealed that GMP/MOL(+) induced 3.4-fold and 3.5-fold stronger tumor apoptosis than GMP(+) and PBS(+), respectively (Figures 5f and S26). These results strongly support synergistic chemoradiotherapy by slowly releasing GMP from GMP/MOL and enhancing RT by the MOL.

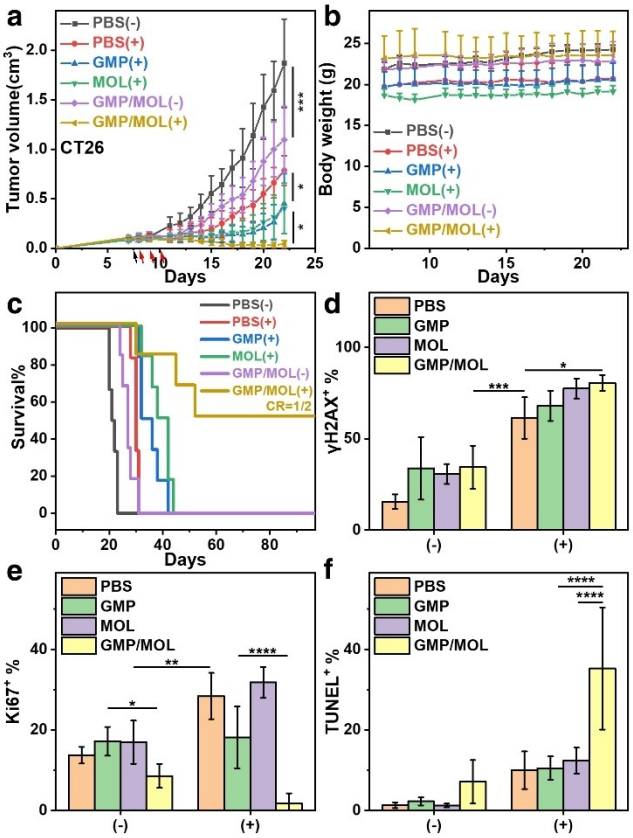

Figure 5. (a) Tumor volumes and (b) body weights of CT26 tumor-bearing BALB/c mice after different treatments ($n=6$, the black arrow indicates *i.t.* injection, and the red arrow indicates X-ray irradiation of 2 Gy for 3 fractions). (c) Survival percentages of mice in different treatment groups up to 97 days after tumor inoculation. (d–f) Quantification of positive cell percentages in IHC staining of (d) γ-H2AX, (e) Ki67, and (f) TUNEL for evaluation of DNA damage, cancer proliferation, and apoptosis, respectively ($n=6$). *$p<0.05$, **$p<0.01$, ***$p<0.001$, ****$p<0.0001$.

In summary, we used a 2D MOL comprising Hf_{12}-SBUs and Ir-based photosensitizing ligands to deliver GMP and enhance radiotherapy. DFT calculations, ITC measurements, phosphate-dependent release, and intratumoral pharmacokinetics studies demonstrated that strong coordination between GMP and Hf_{12}-SBUs prolonged its intratumor retention and triggered its slow release in tumors through a phosphate concentration increase inside cells. Upon low-dose X-ray irradiation, the intrinsic radioenhancement by the MOL synergized with the enhanced chemotherapeutic effect of locally released GMP to significantly inhibit tumor growth with complete tumor eradication in 50 % of mice. This work establishes a new treatment paradigm for combining radiotherapy and chemotherapy with a single nanoparticle.

Acknowledgements

We thank Yingjie Fan for help with ICP-MS and NMR studies. We thank Zitong Wang for help with DFT calculations. We thank Dr. Christine Labno for help with confocal imaging and whole-slide scanning. We thank Dr. Shihong Li, Xin Jiang, Can Gong, and Ming Cheng for help with the histology-related studies. We thank Dr. YuYang Wu for help with solid-state NMR. We thank Dr. Alexander Filatov and Dr. Yi Xie for experimental help. We acknowledge funding from the National Cancer Institute (1R01CA253655) and Chicago Biomedical Consortium and the University of Chicago Medicine Comprehensive Cancer Center (NIH CCSG: P30CA014599).

Conflict of Interest

Wenbin Lin is founder and chairman of Coordination Pharmaceuticals which licenses some of the nanomedicine technologies developed in the Lin lab.

Data Availability Statement

The data that support the findings of this study are available from the corresponding author upon reasonable request.

Keywords: Metal-Organic Layer · Radiotherapy · Chemotherapy · Cancer · Drug Delivery

[1] a) B. A. Chabner, T. G. Roberts, *Nat. Rev. Cancer* **2005**, *5*, 65–72; b) V. T. DeVita Jr., E. Chu, *Cancer Res.* **2008**, *68*, 8643–8653.

[2] a) N. J. Vogelzang, *J. Clin. Oncol.* **1984**, *2*, 1289–1304; b) L. A. Decosterd, N. Widmer, K. Zaman, E. Cardoso, T. Buclin, C. Csajka, *Biomarkers Med.* **2015**, *9*, 887–893.

[3] J. B. Wolinsky, Y. L. Colson, M. W. Grinstaff, *J. Controlled Release* **2012**, *159*, 14–26.

[4] a) A. Morales, D. Eidinger, A. W. Bruce, *J. Urol.* **1976**, *116*, 180–183; b) K. A. Walter, R. J. Tamargo, A. Olivi, P. C. Burger, H. Brem, *Neurosurgery* **1995**, *37*, 1128–1145; c) R. I. Haroun, H. Brem, *Curr. Opin. Oncol.* **2000**, *12*, 187–193.

[5] a) E. P. Goldberg, A. R. Hadba, B. A. Almond, J. S. Marotta, *J. Pharm. Pharmacol.* **2002**, *54*, 159–180; b) C. Y. X. Chua, J. Ho, S. Demaria, M. Ferrari, A. Grattoni, *Adv. Ther.* **2020**, *3*, 2000027.

[6] a) M. Spiotto, Y.-X. Fu, R. R. Weichselbaum, *Sci. Immunol.* **2016**, *1*, eaag1266-eaag1266; b) R. R. Weichselbaum, H. Liang, L. Deng, Y.-X. Fu, *Nat. Rev. Clin. Oncol.* **2017**, *14*, 365–379; c) G. Petroni, L. C. Cantley, L. Santambrogio, S. C. Formenti, L. Galluzzi, *Nat. Rev. Clin. Oncol.* **2022**, *19*, 114–131; d) J. M. Price, A. Prabhakaran, C. M. L. West, *Nat. Rev. Clin. Oncol.* **2023**, *20*, 83–98.

[7] A. C. Begg, F. A. Stewart, C. Vens, *Nat. Rev. Cancer* **2011**, *11*, 239–253.

[8] a) T. Y. Seiwert, J. K. Salama, E. E. Vokes, *Nat. Clin. Pract. Oncol.* **2007**, *4*, 86–100; b) L. Kleinberg, M. K. Gibson, A. A. Forastiere, *Nat. Clin. Pract. Oncol.* **2007**, *4*, 282–294; c) R. R. Weichselbaum, H. Ishwaran, T. Yoon, D. S. A. Nuyten, S. W. Baker, N. Khodarev, A. W. Su, A. Y. Shaikh, P. Roach, B. Kreike, B. Roizman, J. Bergh, Y. Pawitan, M. J. van de Vijver, A. J. Minn, *Proc. Natl. Acad. Sci. USA* **2008**, *105*, 18490–18495; d) K. Kono, K. Mimura, R. Kiessling, *Cell Death Dis.* **2013**, *4*, e688–e688.

[9] a) T. Y. Seiwert, J. K. Salama, E. E. Vokes, *Nat. Clin. Pract. Oncol.* **2007**, *4*, 156–171; b) Y. H. Wang, N. Yao, K. K. Wei, L. Jiang, S. Hanif, Z. X. Wang, C. X. Pei, *Eur. J. Clin. Nutr.* **2016**, *70*, 1246–1253; c) D. De Ruysscher, G. Niedermann, N. G. Burnet, S. Siva, A. W. M. Lee, F. Hegi-Johnson, *Nat. Rev. Dis. Primers* **2019**, *5*, 13; d) J. Mangesius, D. Minasch, K. Fink, M. Nevinny-Stickel, P. Lukas, U. Ganswindt, T. Seppi, *Strahlenther. Onkol.* **2023**, *199*, 67–77.

[10] a) G. Lan, K. Ni, W. Lin, *Coord. Chem. Rev.* **2019**, *379*, 65–81; b) K. Lu, T. Aung, N. Guo, R. Weichselbaum, W. Lin, *Adv. Mater.* **2018**, *30*, 1707634; c) P. Horcajada, R. Gref, T. Baati, P. K. Allan, G. Maurin, P. Couvreur, G. Férey, R. E. Morris, C. Serre, *Chem. Rev.* **2012**, *112*, 1232–1268; d) P. Horcajada, C. Serre, M. Vallet-Regí, M. Sebban, F. Taulelle, G. Férey, *Angew. Chem. Int. Ed.* **2006**, *45*, 5974–5978; e) P. Horcajada, T. Chalati, C. Serre, B. Gillet, C. Sebrie, T. Baati, J. F. Eubank, D. Heurtaux, P. Clayette, C. Kreuz, J.-S. Chang, Y. K. Hwang, V. Marsaud, P.-N. Bories, L. Cynober, S. Gil, G. Férey, P. Couvreur, R. Gref, *Nat. Mater.* **2010**, *9*, 172–178; f) M. Lismont, L. Dreesen, S. Wuttke, *Adv. Funct. Mater.* **2017**, *27*, 1606314; g) R. Freund, O. Zaremba, G. Arnauts, R. Ameloot, G. Skorupskii, M. Dincă, A. Bavykina, J. Gascon, A. Ejsmont, J. Goscianska, M. Kalmutzki, U. Lächelt, E. Ploetz, C. S. Diercks, S. Wuttke, *Angew. Chem. Int. Ed.* **2021**, *60*, 23975–24001; h) R. Ettlinger, U. Lächelt, R. Gref, P. Horcajada, T. Lammers, C. Serre, P. Couvreur, R. E. Morris, S. Wuttke, *Chem. Soc. Rev.* **2022**, *51*, 464–484; i) X. Lian, Y. Fang, E. Joseph, Q. Wang, J. Li, S. Banerjee, C. Lollar, X. Wang, H.-C. Zhou, *Chem. Soc. Rev.* **2017**, *46*, 3386–3401; j) J. Park, Q. Jiang, D. Feng, L. Mao, H.-C. Zhou, *J. Am. Chem. Soc.* **2016**, *138*, 3518–3525; k) W. Wang, Y. Yu, Y. Jin, X. Liu, M. Shang, X. Zheng, T. Liu, Z. Xie, *J. Nanobiotechnol.* **2022**, *20*, 207; l) L. Wang, M. Zheng, Z. Xie, *J. Mater. Chem. B* **2018**, *6*, 707–717; m) V. Rodriguez-Ruiz, A. Maksimenko, R. Anand, S. Monti, V. Agostoni, P. Couvreur, M. Lampropoulou, K. Yannakopoulou, R. Gref, *J. Drug Targeting* **2015**, *23*, 759–767; n) X. Li, E. Porcel, M. Menendez-Miranda, J. Qiu, X. Yang, C. Serre, A. Pastor, D. Desmaële, S. Lacombe, R. Gref, *ChemMedChem* **2020**, *15*, 274–283.

[11] a) K. Lu, C. He, N. Guo, C. Chan, K. Ni, G. Lan, H. Tang, C. Pelizzari, Y.-X. Fu, M. T. Spiotto, R. R. Weichselbaum, W. Lin, *Nat. Biomed. Eng.* **2018**, *2*, 600–610; b) Z. Huang, Y. Wang, D. Yao, J. Wu, Y. Hu, A. Yuan, *Nat. Commun.* **2021**, *12*, 145; c) F. Hao, Z.-Y. Yan, X.-P. Yan, *Small Sci.* **2022**, *2*, 2200044; d) K. Ni, G. Lan, W. Lin, *ACS Cent. Sci.* **2020**, *6*, 861–868; e) Z. Xu, K. Ni, J. Mao, T. Luo, W. Lin, *Adv. Mater.* **2021**, *33*, 2104249.

[12] a) L. Cao, Z. Lin, W. Shi, Z. Wang, C. Zhang, X. Hu, C. Wang, W. Lin, *J. Am. Chem. Soc.* **2017**, *139*, 7020–7029; b) G. Lan, K. Ni, S. S. Veroneau, Y. Song, W. Lin, *J. Am. Chem. Soc.* **2018**, *140*, 16971–16975; c) G. Lan, Y. Quan, M. Wang, G. T. Nash, E. You, Y. Song, S. S. Veroneau, X. Jiang, W. Lin, *J. Am. Chem. Soc.* **2019**, *141*, 15767–15772; d) T. Luo, Y. Fan, J. Mao, E. Yuan, E. You, Z. Xu, W. Lin, *J. Am. Chem. Soc.* **2022**, *144*, 5241–5246.

[13] a) W. Shi, L. Cao, H. Zhang, X. Zhou, B. An, Z. Lin, R. Dai, J. Li, C. Wang, W. Lin, *Angew. Chem. Int. Ed.* **2017**, *56*, 9704–9709; b) Y. Quan, G. Lan, Y. Fan, W. Shi, E. You, W. Lin, *J. Am. Chem. Soc.* **2020**, *142*, 1746–1751; c) T. Luo, G. T. Nash, X. Jiang, X. Feng, J. Mao, J. Liu, A. Juloori, A. T. Pearson, W. Lin, *Adv. Mater.* **2022**, *34*, 2110588; d) T. Luo, Y. Fan, J. Mao, X. Jiang, L. Albano, E. Yuan, T. Germanas, W. Lin, *Angew.*

Chem. Int. Ed. **2023**, e202301910; e) A. Wang, K. Barcus, S. M. Cohen, *J. Am. Chem. Soc.* **2023**, *145*, 16821–16827.
[14] a) D. B. Longley, D. P. Harkin, P. G. Johnston, *Nat. Rev. Cancer* **2003**, *3*, 330–338; b) N. J. Mullen, P. K. Singh, *Nat. Rev. Cancer* **2023**.
[15] a) B. Reif, S. E. Ashbrook, L. Emsley, M. Hong, *Nat. Rev. Methods Primers* **2021**, *1*, 2; b) M. P. Foster, C. A. McElroy, C. D. Amero, *Biochemistry* **2007**, *46*, 331–340.
[16] a) P. Kohli, G. J. Blanchard, *Langmuir* **2000**, *16*, 695–701; b) Z. Wang, Y. Fu, Z. Kang, X. Liu, N. Chen, Q. Wang, Y. Tu, L. Wang, S. Song, D. Ling, H. Song, X. Kong, C. Fan, *J. Am. Chem. Soc.* **2017**, *139*, 15784–15791.
[17] a) J. P. Knochel, R. Haller, E. Ferguson, in *Phosphate and Minerals in Health and Disease* (Eds.: S. G. Massry, E. Ritz, H. Jahn), Springer US, Boston, MA **1980**, pp. 323–334; b) J. W. Bowen, C. Levinson, *J. Cell. Physiol.* **1982**, *110*, 149–154; c) C. Auesukaree, T. Homma, H. Tochio, M. Shirakawa, Y. Kaneko, S. Harashima, *J. Biol. Chem.* **2004**, *279*, 17289–17294; d) M. Goretti Pinedo, U. S. Alon, *Pediatr. Nephrol.* **2017**, *32*, 1999–1999; e) G. Chazot, S. Lemoine, G. Kocevar, E. Kalbacher, D. Sappey-Marinier, O. Rouvière, L. Juillard, *J. Am. Soc. Nephrol.* **2021**, *32*, 229–237.
[18] G. T. Nash, T. Luo, G. Lan, K. Ni, M. Kaufmann, W. Lin, *J. Am. Chem. Soc.* **2021**, *143*, 2194–2199.
[19] Z. Xu, T. Luo, W. Lin, *Acc. Mater. Res.* **2021**, *2*, 944–953.

Manuscript received: December 27, 2023
Accepted manuscript online: February 21, 2024
Version of record online: ■■, ■■

Communications

Chemoradiotherapy

T. Luo, X. Jiang, J. Li, G. T. Nash, E. Yuan, L. Albano, L. Tillman, W. Lin* _____ e202319981

Phosphate Coordination to Metal-Organic Layer Secondary Building Units Prolongs Drug Retention for Synergistic Chemoradiotherapy

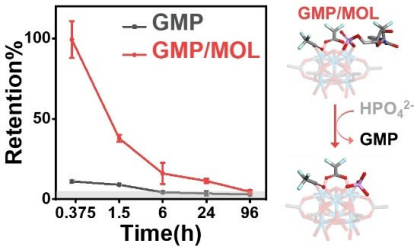

Coordination of gemcitabine monophosphate (GMP) to a nanoscale metal-organic layer (MOL) prolongs its intratumoral retention and allows its continuous release for effective localized chemotherapy. Under low-dose X-ray irradiation, GMP-loaded MOL (GMP/MOL) significantly outperforms free GMP and provides synergistic, potent chemoradiotherapy without causing side effects.